

$NiO/\beta\text{-}Ga_2O_3$ heterojunction diodes with ultra-low leakage current below 10^{-10} A and high thermostability

Yi Huang(黄义), Wen Yang(杨稳), Qi Wang(王琦), Sheng Gao(高升), Wei-Zhong Chen(陈伟中), Xiao-Sheng Tang(唐孝生), Hong-Sheng Zhang(张红升), and Bin Liu(刘斌)

Citation: Chin. Phys. B, 2023, 32 (**9**): 098502. DOI: 10.1088/1674-1056/aca4be
Journal homepage: http://cpb.iphy.ac.cn; http://iopscience.iop.org/cpb

What follows is a list of articles you may be interested in

An insulated-gate bipolar transistor model based on the finite-volume charge method

Manhong Zhang(张满红) and Wanchen Wu(武万琛)
Chin. Phys. B, 2022, 31 (**12**): 128501. DOI: 10.1088/1674-1056/ac8723

Effect of temperature on photoresponse properties of solar-blind Schottky barrier diode photodetector based on single crystal Ga_2O_3

Chao Yang(杨超), Hongwei Liang(梁红伟), Zhenzhong Zhang(张振中), Xiaochuan Xia(夏晓川), Heqiu Zhang(张贺秋), Rensheng Shen(申人升), Yingmin Luo(骆英民), Guotong Du(杜国同)
Chin. Phys. B, 2019, 28 (**4**): 048502. DOI: 10.1088/1674-1056/28/4/048502

Photovoltaic effects in reconfigurable heterostructured black phosphorus transistors

Siqi Hu(胡思奇), Ruijuan Tian(田睿娟), Xiaoguang Luo(罗小光), Rui Yin(殷瑞), Yingchun Cheng(程迎春), Jianlin Zhao(赵建林), Xiaomu Wang(王肖沐), Xuetao Gan(甘雪涛)
Chin. Phys. B, 2018, 27 (**12**): 128502. DOI: 10.1088/1674-1056/27/12/128502

Improved performance of Ge n^+/p diode by combining laser annealing and epitaxial Si passivation

Chen Wang(王尘), Yihong Xu(许怡红), Cheng Li(李成), Haijun Lin(林海军)
Chin. Phys. B, 2018, 27 (**1**): 018502. DOI: 10.1088/1674-1056/27/1/018502

AlGaN/GaN high-electron-mobility transistor with transparent gate by Al-doped ZnO

Wang Chong (王冲), He Yun-Long (何云龙), Zheng Xue-Feng (郑雪峰), Ma Xiao-Hua (马晓华), Zhang Jin-Cheng (张进成), Hao Yue (郝跃)
Chin. Phys. B, 2013, 22 (**6**): 068503. DOI: 10.1088/1674-1056/22/6/068503

NiO/β-Ga_2O_3 heterojunction diodes with ultra-low leakage current below 10^{-10} A and high thermostability

Yi Huang(黄义)[1], Wen Yang(杨稳)[1], Qi Wang(王琦)[1,†], Sheng Gao(高升)[1], Wei-Zhong Chen(陈伟中)[1], Xiao-Sheng Tang(唐孝生)[1], Hong-Sheng Zhang(张红升)[1], and Bin Liu(刘斌)[2]

[1] *School of Optoelectronic Engineering, Chongqing University of Posts and Telecommunications, Chongqing* 400065, *China*
[2] *School of Electronic Science and Engineering, Nanjing University, Nanjing* 210093, *China*

(Received 15 October 2022; revised manuscript received 16 November 2022; accepted manuscript online 22 November 2022)

The 10 nm p-NiO thin film is prepared by thermal oxidation of Ni on β-Ga_2O_3 to form NiO/β-Ga_2O_3 p–n heterojunction diodes (HJDs). The NiO/β-Ga_2O_3 HJDs exhibit excellent electrostatic properties, with a high breakdown voltage of 465 V, a specific on-resistance ($R_{on,sp}$) of 3.39 mΩ·cm^2, and a turn-on voltage (V_{on}) of 1.85 V, yielding a static Baliga's figure of merit (FOM) of 256 MW/cm^2. Also, the HJDs have a low turn-on voltage, which reduces conduction loss dramatically, and a rectification ratio of up to 10^8. Meanwhile, the HJDs' reverse leakage current is essentially unaffected at temperatures below 170 °C, and their leakage level may be controlled below 10^{-10} A. This indicates that p-NiO/β-Ga_2O_3 HJDs with good thermal stability and high-temperature operating ability can be a good option for high-performance β-Ga_2O_3 power devices.

Keywords: NiO/β-Ga_2O_3 p–n heterojunction diodes, Baliga's figure of merit, reverse leakage current, β-Ga_2O_3 power devices

PACS: 85.30.Kk, 73.40.Lq, 81.05.Hd **DOI:** 10.1088/1674-1056/aca4be

1. Introduction

Beta-phase gallium oxide (β-Ga_2O_3) shows great potential as a high-power device material. It is predicted to become a research hotspot for the next generation due to its ultra-wide bandgap and high critical electric field (8 MV/cm), superior to SiC and GaN.[1–4] The unipolar- and bipolar-power devices based on β-Ga_2O_3 have high application value in electronic circuits.[5] One notable potential market is in the applications of power converters, inverters, and power supplies for servers.[6–8] However, the difficulty in realizing p-type β-Ga_2O_3 is still an obstacle to realizing advanced bipolar power devices in practical applications. It could be an alternative choice to construct heterojunctions by employing other p-type oxide materials on β-Ga_2O_3.[5,9] In the p-type oxide family, wide bandgap NiO materials can be used for integration with n-Ga_2O_3 due to their high-visible spectral transparency and p-type conductivity derived from nickel vacancies or monovalent impurities.[10] He *et al*. successfully achieved selective high-resistance zones on β-Ga_2O_3 wafers, which considerably reduced the leakage current and increased the breakdown voltage of Schottky barrier diodes (SBD).[11] Xiong *et al*. reported a β-Ga_2O_3 double-barrier Schottky barrier diode (DBSBD) with a low turn-on voltage of 1.13 V and low reverse leakage current of 1.27×10^{-7} A/cm^2 (at -100 V).[12] Recently, NiO/Ga_2O_3 HJDs have been proven to have excellent reverse blocking ability. Lu *et al*. reported a vertical NiO/β-Ga_2O_3 heterojunction diode by sputtering a layer of NiO thin film on β-Ga_2O_3 substrate, and its breakdown voltage (V_{BR}) exceeded 1 kV.[13] Xu *et al*. demonstrated an effective edge termination for vertical NiO/β-Ga_2O_3 heterojunction diodes using a continuous p-NiO film as a junction termination extension (JTE), which increased the I_{on}/I_{off} ratio up to $\sim 10^{10}$ A and achieved a high breakdown voltage of 2.66 kV.[14] Gong *et al*. reported a double-layered NiO/β-Ga_2O_3 p–n heterojunction diode and obtained a 1.86 kV high breakdown voltage (B_V) and low reverse leakage current below 1 μA/cm^2.[10] In recent years, NiO/β-Ga_2O_3 HJDs have achieved a high breakdown voltage of nearly 2 kV, but most of them have high reverse leakage current under high reverse bias voltage. And the changes in electrical properties such as voltage, on-resistance and reverse leakage current of various devices under high temperature and variable temperature still need further study.

In this work, the NiO/β-Ga_2O_3 HJDs are prepared with 10 nm thick p-NiO prepared by thermal oxidation of Ni on the β-Ga_2O_3. The breakdown voltage is as high as 465 V, and excellent forward and reverse output characteristics are obtained. The output characteristics of the HJDs under different temperatures are tested. It is found that the reverse leakage current of the HJDs is basically unchanged and the variation range is between 10^{-11}–10^{-10} A. Meanwhile, the leakage current can be maintained below 10^{-10} A, and the high-temperature resistance of the devices is excellent. This paper, thus, further confirms the potential of Ga_2O_3 HJDs for high power, high temperature, and high-reliability applications.[15–17]

†Corresponding author. E-mail: wangqi@cqupt.edu.cn

© 2023 Chinese Physical Society and IOP Publishing Ltd

2. Device fundamentals

Figure 1(a) shows a schematic cross-section of a vertical NiO/β-Ga_2O_3 HJD on a highly conductive Sn-doped (001) β-Ga_2O_3 substrate with an electron concentration of 1.5×10^{19} cm^{-3}. The 6 μm Si-doped β-Ga_2O_3 drift region was grown by hydride vapor phase epitaxy. The doping concentration was measured by Hall measurement at room temperature to be 2×10^{16} cm^{-3}. Firstly, the 30/150 nm Ti/Au was deposited by electron beam evaporation to form a backside ohmic contact (cathode), followed by rapid thermal annealing at 480 °C for 1 min under a N_2 ambient. After the lithography, the metal Ni was evaporated at the heterojunction in the drift region, followed by oxidation at 400 °C for 20 min. The Ni was oxidized to create 10 nm thick NiO to form a p-NiO layer. The thickness of the p-type NiO is measured by atomic force microscope. The Hall measurement characterizations of the p-NiO film indicate that the 10-nm-thick layer has hole concentrations of 1.33×10^{18} cm^{-3}. Finally, a Ni/Au (200/150 nm) layer was deposited on the NiO layer as a metal anode. Meanwhile, the Ni/β-Ga_2O_3 SBD was also manufactured on the same chip using identical processes. Figure 1(b) is the SEM anode surface image of the HJD, and the diameter of the metal anode is 150 μm. The energy band diagram of the p-NiO/β-Ga_2O_3 heterojunction is shown in Fig. 1(c).

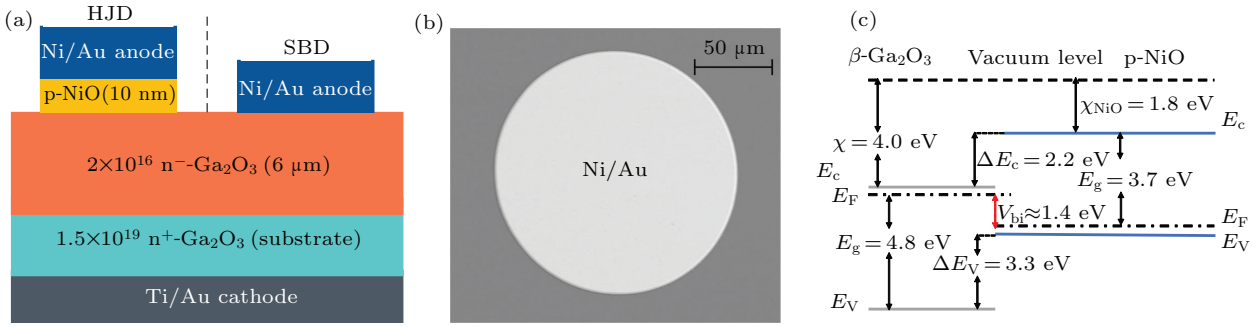


Fig. 1. (a) Schematic cross-section of a vertical NiO/β-Ga_2O_3 HJD (left) and Ni/β-Ga_2O_3 SBD (right). (b) SEM anode surface image of an HJD. (c) Schematic energy band diagram of a NiO/β-Ga_2O_3 p–n heterojunction.

3. Results and discussion

The electrical properties of the devices are tested by a B1505A power device analyzer in the DC mode. The forward output curve of the HJD and SBD are shown in Fig. 2(a), from which it can be seen that the turn-on voltage of the HJD and SBD are 1.85 V and 0.77 V respectively. Compared to conventional p–n junction diodes, HJDs possess certain performance advantages, including low turn-on voltages. By fitting the linear region of the output curve, it is calculated that the specific on-resistances of the HJD and SBD are 3.39 mΩ·cm^2 and 2.77 mΩ·cm^2, which are far lower than that of the conventional β-Ga_2O_3 SBD.[18] It can be seen from Fig. 2(a) that the on/off current ratios of the HJD and SBD are as high as 10^8. As shown in Fig. 2(b), the $R_{on,sp}$ of the HJD increases $\sim$ 1.35 mΩ·cm^2 as the temperature (T) rises from 30 °C to 140 °C and then stabilizes at 4.75 mΩ·cm^2. The Ga_2O_3 HJD exhibits T-independent $R_{on,sp}$ behavior similar to as in GaN p–n diodes.[19] Additionally, due to the bandgap narrowing effect and thermally-enhanced carrier diffusion,[5] the value of V_{on} reduces from 1.85 V to 1.55 V with elevated temperatures. And the value of V_{on} reduces from 0.77 V to 0.55 V.

The reverse breakdown characteristics of the HJD and SBD are shown in Fig. 2(d). The breakdown voltages of the HJD and SBD are 465 V and 302.7 V respectively, and the Baliga's FOM of the HJD is calculated to be 256 MW/cm^2. The HJD presents optimal reverse current suppression capabilities when suffering from a reverse bias voltage of below 175 V to a reverse leakage current of less than 10^{-9} A. Above 175 V, the HJD retains a leakage current of 10^{-8} A, demonstrating its more remarkable reverse suppression capacity than the SBD. The leakage current of the HJD may be sustained at below 10^{-10} A when the reverse voltage is less than 100 V, while the leakage current of the SBD is above 10^{-10} A, and the HJD obtains a leakage current of 10^{-11} A at a bias voltage of less than 60 V, which is shown in Fig. 2(c). The HJDs present good reverse blocking performance. Compared with the β-Ga_2O_3-based HJD fabricated by magnetron sputtering, the HJDs fabricated by thermal oxidation have superior stabilities and performance consistencies, laying a technological foundation for the preparation of high-performance Ga_2O_3-based devices.

To explore the temperature resistance characteristics of the device, the leakage current is tested under a 100 V reverse bias voltage. As shown in Fig. 3(a), the device still maintains good reverse suppression performance at a temperature of 30 °C–140 °C. The reverse leakage current of the HJD is basically unchanged below 140 °C, which is similar to that at room temperature. Figure 3(b) shows that the reverse leakage current of the HJD at 170 °C is lower than one order of magnitude different from that at room temperature. Meanwhile, the reverse leakage current of the SBD increases at 140 °C and 170 °C, which is shown in Figs. 3(a) and 3(b). The β-Ga_2O_3 HJD shows good thermal stability and reliable performance at high temperatures.

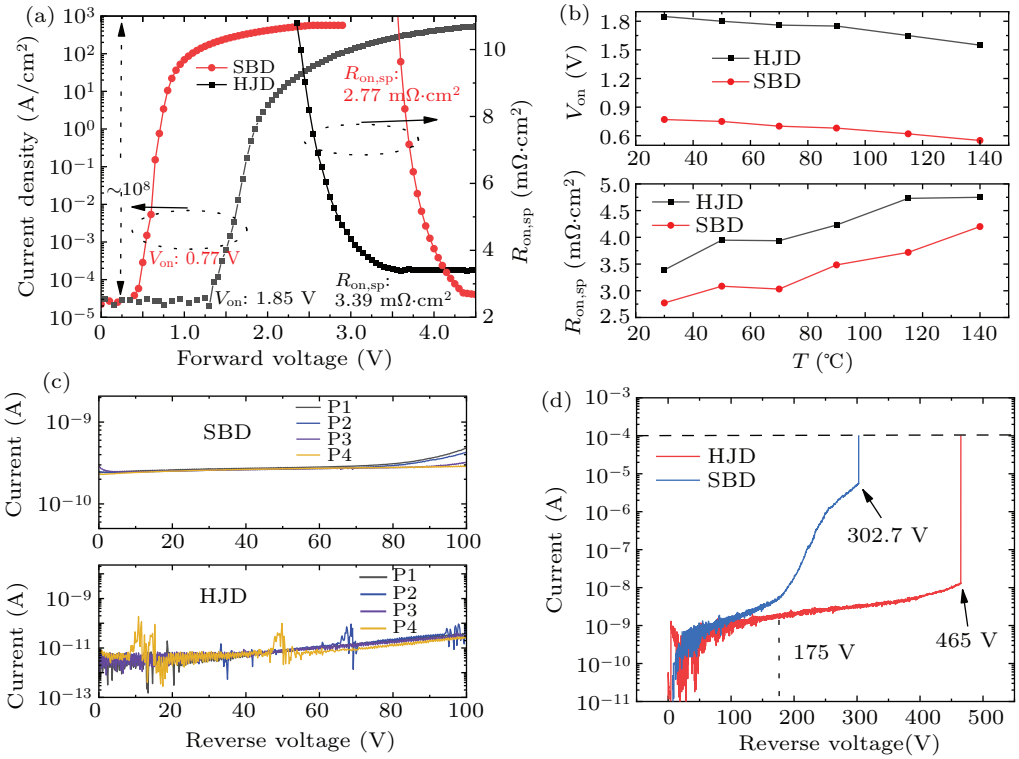


Fig. 2. (a) The logarithmic curve of the forward characteristics of the HJD and SBD. (b) Forward temperature test curve of the HJD and SBD. (c) Test curve of HJDs and SBDs under 100 V reverse bias voltage. (d) The logarithmic curve of the reverse breakdown characteristics of the HJD and SBD.

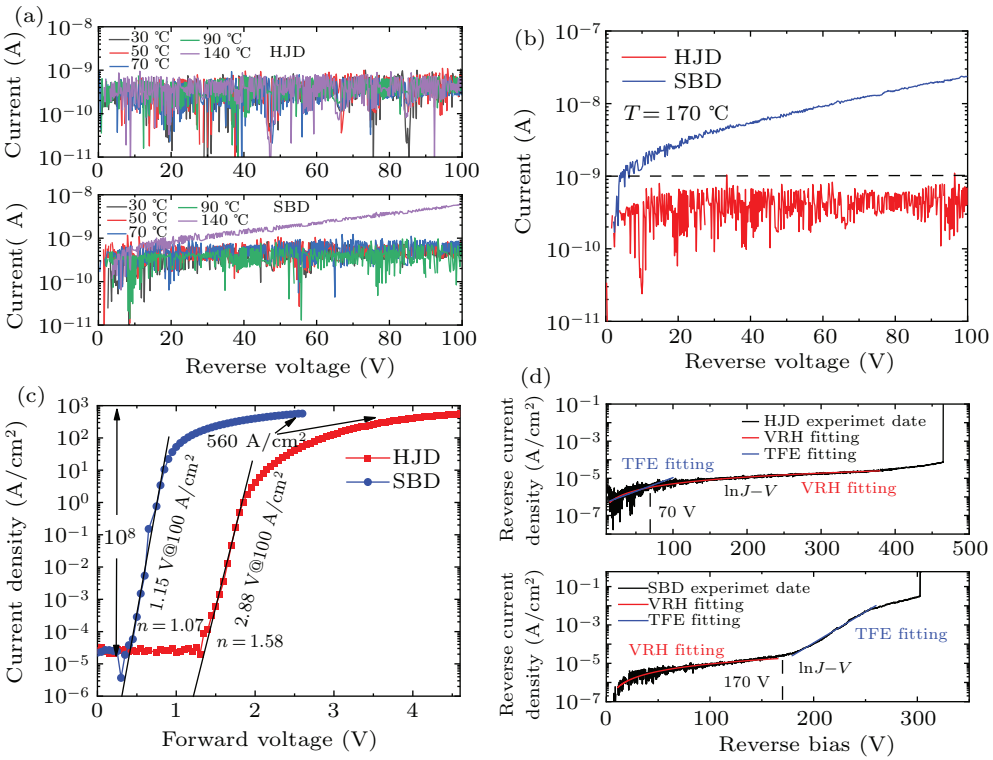


Fig. 3. (a) The test curve of the HJD and SBD under 100 V reverse bias and 30 °C–140 °C variable temperature. (b) The test curve of the HJD and SBD under 100 V reverse bias and 170 °C high temperature. (c) The logarithmic curve of the forward characteristics of the HJD and SBD. (d) ln(J)–V curve of the reverse characteristics of the HJD and SBD.

The four current transport processes of the device are analyzed. In the case of minimal current injection, the electron–hole complexation process in the space charge region dominates and exhibits complex current domination. And the current magnitude is proportional to $\exp(qV_A/(2k_BT))$. When the current gradually increases to a certain degree, the device exhibits a low current injection process, in which the concentration of minority carriers injected into the drift region is

much lower than the doping concentration in the drift region. The minority carrier diffusion process in the drift region dominates and exhibits a diffusion current, at which time the current magnitude is proportional to $\exp(qV_A/(k_BT))$. When the concentration of injected minority carriers in the drift region exceeds the doping concentration in the drift region, the device reaches a high current injection process. The current transport depends on the high concentration of electrons and holes in the drift region, and the current magnitude is proportional to $\exp(qV_A/(2k_BT))$. When the device's forward current reaches a greater current density, the compounding effect in the end region reduces the carrier concentration injected into the drift region, which makes the forward voltage drop of the device increase and the device output current gradually tends to saturation. Cheung and Zhou *et al.*[20,21] have proposed that when the voltage $V_D = V_A - JAR_S > 3k_BT/e$ (~ 0.08 V) is applied to the diode, the relationship between device voltage V_A and current density J can be simplified as

$$V_A = JAR_S + n\Phi_B + \frac{nk_BT}{e}\ln\left[\frac{J}{A^*T^2}\right]. \tag{1}$$

Solving the differential equation of V_A about $\ln J$, we can get

$$\frac{d(V_A)}{d(\ln J)} = JAR_S + \frac{nk_BT}{e}, \tag{2}$$

where e, A, R_S, n, k_B, T, A^*, and are the elementary charge, device area, series resistance, ideality factor, Boltzmann constant, temperature, effective Richardson constant, and Schottky barrier height at equilibrium (zero bias), respectively. The logarithmic curve of the HJD's and SBD's positive properties are shown in Fig. 3(c). The HJD has a high rectifier ratio of 10^8. Under the positive output constraint, both the HJD and SBD reach an output current density of 560 A/cm^2. The output current density of the HJD and SBD exceeds 100 A/cm^2 at 2.88 V and 1.15 V respectively. The ideality factor extracted from the fitting curve slope is 1.58 (HJD) and 1.07 (SBD). It can be concluded that the forward conduction current of the HJD is mainly compound current and diffusion current, while the forward conduction current of the SBD is mainly diffusion current.

The reverse leakage mechanism in Ga_2O_3-based vertical structure power diode devices is commonly explained using two methods: the thermionic-field emission (TFE) mechanism and variable range hopping conduction (VRH). According to the thermal electron field emission mechanism, formula (2) can be transposed and simplified as follows:

$$\ln J = \frac{e}{nk_BT}V_A + \ln A^*T^2 - \frac{ef_B}{k_BT}. \tag{3}$$

For variable range hopping, the leakage current is expressed as follows:[22]

$$J = J_0\exp\left(\frac{CE}{2k_BT}\left(\frac{T_0}{T}\right)^{\frac{1}{4}}\right), \tag{4}$$

with

$$E = (V_{bi} - V_r)/W_d, \tag{5}$$

where, C, E, V_{bi}, and W_d are the constant, the electric field, the built-in potential, and the thickness of the drift region, respectively. The dependence of J and E is $\ln(J) \propto E$, and the slope of the $\ln(J)$–$\ln(E)$ fitting curve is close to 1. Figure 3(d) shows the $\ln(J)$–V curve of the HJD and SBD after fitting the double logarithm curve. Through fitting analysis, the variable range jump conduction mechanism of the HJD can completely fit the whole leakage current curve, which clearly explains the mechanism of leakage current generation. Figure 4(a) shows the two-dimensional electric field distribution at a reverse bias of 500 V for the HJD, using Silvaco TCAD software. Electric field profiles along the cutline at the device edge have been extracted and are shown in Fig. 4(b). The peak electric field of the HJD reaches the value of 7.9 MV/cm. The magnitude of the peak electric field for the HJD device has almost reached the theoretical Ga_2O_3 breakdown electric field (8 MV/cm).

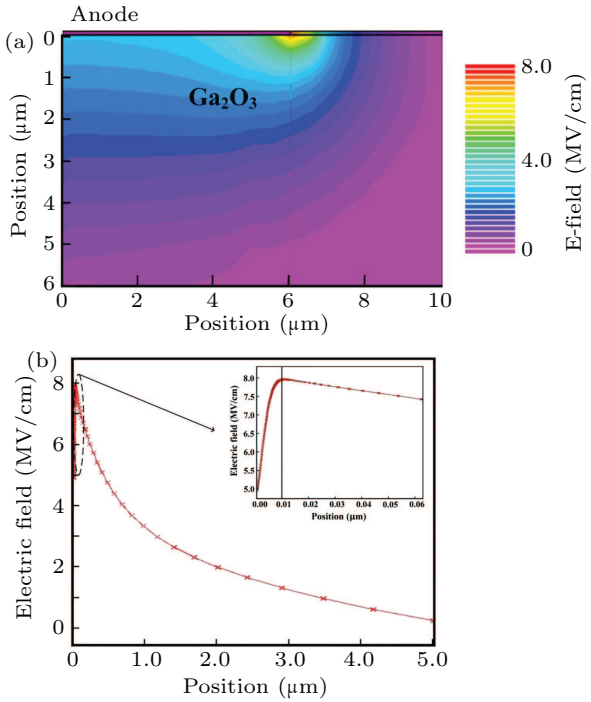


Fig. 4. (a) Two-dimensional electric field distributions at a reverse bias of 500 V of the HJD device simulated by Silvaco TCAD software. (b) Extracted electric field profiles along the cutline at the device edges of the HJD device.

4. Conclusion

In summary, β-Ga_2O_3 HJDs with p-NiO prepared by thermal oxidation processes are studied. The high breakdown

voltage (465 V), turn-on voltage (1.85 V), and low specific on-resistance (3.39 mΩ·cm^2) of the HJD are obtained. The HJD structure efficiently reduces conduction loss and improves electrical performance. Moreover, the performance of the HJD is equivalent to that of an HJD formed by magnetron sputtering. The reverse leakage current of NiO/β-Ga_2O_3 HJDs can always remain around 10^{-10} A when the temperature varies from 30 °C to 140 °C, indicating that Ga_2O_3 HJDs have great practical potential for high-temperature, high-power, and high-reliability applications.

Acknowledgements

Project supported by the Technology Innovation and Application Demonstration Key Project of Chongqing Municipality (cstc2019jszx-zdztzxX0005), the Technology Innovation and Application Demonstration Key Project of Chongqing Municipality (cstc2020jscx-gksbX0011), the Science and Technology Research Program of Chongqing Municipal Education Commission (KJQN202100614), and the Natural Science Foundation of Chongqing (cstc2021jcyj-bshX0146).

References

[1] Hao W B, He Q, Zhou K, Xu G, Xiong W, Zhou X, Jian G, Chen C, Zhao X and Long S 2021 *Appl. Phys. Lett.* **118** 043501
[2] Ji M, Taylor N R, Kravchenko I, Joshi P, Aytug T, Cao L R and Paranthaman M P 2021 *IEEE Trans. Power Electron.* **36** 41
[3] Pearton S J, Yang J, Cary P H, Ren F, Kim J, Tadjer M J and Mastro M A 2018 *Appl. Phys. Rev.* **5** 011301
[4] Xiao M, Wang B, Liu J, Zhang R, Zhang Z, Ding C, Lu S, Sasaki K, Lu G Q, Buttay C and Zhang Y 2021 *IEEE Trans. Power Electron.* **36** 8565
[5] Gong H, Zhou F, Xu W, Yu X, Xu Y, Yang Y, Ren F F, Gu S, Zheng Y, Zhang R, Lu H and Ye J 2021 *IEEE Trans. Power Electron.* **36** 12213
[6] Allen N, Xiao M, Yan X, Sasaki K, Tadjer M J, Ma J, Zhang R, Wang H and Zhang Y 2019 *IEEE Electron. Device. Lett.* **40** 1399
[7] Sharma R, Xian M, Fares C, Law M E, Tadjer M, Hobart K D, Ren F and Pearton S J 2021 *J. Vac. Sci. Technol. A* **39** 013406
[8] Zhang H, Yuan L, Tang X, Hu J, Sun J, Zhang Y, Zhang Y and Jia R 2020 *IEEE Trans. Power Electron.* **35** 5157
[9] Luo H, Zhou X, Chen Z, Pei Y, Lu X and Wang G 2021 *IEEE Trans. Electron. Devices* **68** 3991
[10] Gong H H, Chen X H, Xu Y, Ren F F, Gu S L and Ye J D 2020 *Appl. Phys. Lett.* **117** 022104
[11] He Q, Zhou X, Li Q, Hao W, Liu Q, Han Z, Zhou K, Chen C, Peng J, Xu G, Zhao X, Wu X and Long S 2022 *IEEE Electron. Device. Lett.* **43** 1933
[12] Xiong W, Zhou X, Xu G, He Q, Jian G, Chen C, Yu Y, Hao W, Xiang X, Zhao X, Mu W, Jia Z, Tao X and Long S 2021 *IEEE Electron. Device. Lett.* **42** 430
[13] Lu X, Zhou X, Jiang H, Ng K W, Chen Z, Pei Y, Lau K M and Wang G 2020 *IEEE Electron. Device. Lett.* **41** 449
[14] Hao W B, He Q M, Zhou X Z, Zhao X L, Xu G W and Long S B 2022 *IEEE* 34*th International Symposium on Power Semiconductor Devices and ICs (ISPSD)* pp. 105–108
[15] Gong H H, Yu X X, Xu Y, Chen X H, Kuang Y, Lv Y J, Yang Y, Ren F F, Feng Z H, Gu S L, Zheng Y D, Zhang R and Ye J D 2021 *Appl. Phys. Lett.* **118** 202102
[16] Wang C, Gong H, Lei W, Cai Y, Hu Z, Xu S, Liu Z, Feng Q, Zhou H, Ye J, Zhang J, Zhang R and Hao Y 2021 *IEEE Electron. Device. Lett.* **42** 485
[17] Zhou F, Gong H, Xu W, Yu X, Xu Y, Yang Y, Ren F F, Gu S, Zheng Y, Zhang R, Ye J and Lu H 2022 *IEEE Trans. Power Electron.* **37** 1223
[18] Zhou H, Feng Q, Ning J, Zhang C, Ma P, Hao Y, Yan Q, Zhang J, Lv Y, Liu Z, Zhang Y, Dang K, Dong P and Feng Z 2019 *IEEE Electron. Device. Lett.* **40** 1788
[19] Han S W, Yang S, Li Y K, Liu Y X, and Sheng K 2019 *31st International Symposium on Power Semiconductor Devices and ICs (ISPSD)* pp. 63–66
[20] Lu X, Zhou L D, Chen L, Ouyang X P, Tang H L, Liu B and Xu J 2019 *ECS J. Solid State SC* **8** Q3036
[21] Zhou L D, Lu X, Chen L, Ouyang X P, Liu B, Xu J and Tang H L 2019 *ECS J Solid State SC* **8** Q3054
[22] Zhang Y, Wong H Y, Sun M, Joglekar S, Yu L, Braga N A, R V and Mickevicius T 2015 *Palacios 2015 61st IEEE International Electron Devices Meeting* pp. 35-1